U.S. ARMY COMBAT CAPABILITIES DEVELOPMENT COMMAND
CHEMICAL BIOLOGICAL CENTER

ABERDEEN PROVING GROUND, MD 21010-5424

DEVCOM CBC-TR-1809

Standoff Raman Semi-Collimated (SORSC) Instrument Evaluation: A Comparison to a Traditional Handheld Raman Instrument

Eric R. Languirand

RESEARCH AND TECHNOLOGY DIRECTORATE

February 2023

Disclaimer

The findings in this report are not to be construed as an official Department of the Army position unless so designated by other authorizing documents.

REPORT DOCUMENTATION PAGE

1. REPORT DATE	2. REPORT TYPE	3. DATES COVERED	
		START DATE	END DATE
XX-02-2023	Final	Jan 2020	Feb 2021

4. TITLE AND SUBTITLE
Standoff Raman Semi-Collimated (SORSC) Instrument Evaluation: A Comparison to a Traditional Handheld Raman Instrument

5a. CONTRACT NUMBER	5b. GRANT NUMBER	5c. PROGRAM ELEMENT NUMBER
5d. PROJECT NUMBER	**5e. TASK NUMBER**	**5f. WORK UNIT NUMBER**

6. AUTHOR(S)
Languirand, Eric R.

7. PERFORMING ORGANIZATION NAME(S) AND ADDRESS(ES)
Director, DEVCOM CBC, ATTN: FCDD-CBR-CP, APG, MD 21010-5424

8. PERFORMING ORGANIZATION REPORT NUMBER
DEVCOM CBC-TR-1809

9. SPONSORING/MONITORING AGENCY NAME(S) AND ADDRESS(ES)
U.S. Army Combat Capabilities Development Command Chemical Biological Center, Seedling Program; 8198 Blackhawk Road, Aberdeen Proving Ground, MD 21010-5424

10. SPONSOR/MONITOR'S ACRONYM(S)
DEVCOM CBC

11. SPONSOR/MONITOR'S REPORT NUMBER(S)

12. DISTRIBUTION/AVAILABILITY STATEMENT
Approved for public release: distribution unlimited.

13. SUPPLEMENTARY NOTES
Funding was provided by the Director, DEVCOM CBC under the authorities and provisions of Section 2363 of the FY20 National Defense Authorization Act to develop new technologies, engineer innovations, and introduce game-changing capabilities.

14. ABSTRACT
A non-lens-based, semi-collimated handheld Raman instrument was compared to a traditional lens-based, fixed-focal-length handheld Raman instrument. The semi-collimated handheld Raman instrument provided greater flexibility in distance requirements, as the area under the Raman curve of a polytetrafluoroethylene peak was greater when normalized and compared (as figures of merit) at all distances from 0 to 3 m. A decrease in Raman signal was found to be $1/d^{1.3}$ (where d is distance), which is significantly improved from the traditional $1/d^2$ distance dependence of signal loss. Angle dependence of the Raman signal captured from the instruments was found to be more sensitive for the semi-collimated handheld Raman instrument at 1 m but was comparable to traditional handheld systems at other distances. Finally, it is shown that simulated dissemination patterns could be printed on copy paper and used as surrogates to show how well a system could perform in overlapping and detecting a dispersed surface sample.

15. SUBJECT TERMS

Handheld Raman	Semi-collimated Raman	Raman spectroscopy	Angle dependence
Lens-less Raman	Standoff Raman	Distance dependence	Comparative assessment

16. SECURITY CLASSIFICATION OF:			17. LIMITATION OF ABSTRACT	18. NUMBER OF PAGES
a. REPORT	b. ABSTRACT	C. THIS PAGE		
U	U	U	UU	32

19a. NAME OF RESPONSIBLE PERSON	19b. PHONE NUMBER *(Include area code)*
Renu B. Rastogi	(410) 436-7545

STANDARD FORM 298 (REV. 5/2020)
Prescribed by ANSI Std. Z39.18

Blank

PREFACE

The work described in this report was authorized and funded through FY20 Section 2363 of the National Defense Authorization Act. The work was started in January 2020 and completed in February 2021.

The use of either trade or manufacturers' names in this report does not constitute an official endorsement of any commercial products. This report may not be cited for purposes of advertisement.

This report has been approved for public release.

Acknowledgment

The author acknowledges Dr. Hermes Huang of Smiths Detection (Edgewood, MD) for their generous support in lending the semi-collimated Raman spectrometer prototype for this work.

Blank

EXECUTIVE SUMMARY

A unique handheld standoff Raman detector that uses no focusing optics and has a semi-collimated interrogation source was compared to traditional handheld Raman spectrometers. These instruments provide Warfighters with greater lethality and increase survivability by allowing them to address potential chemical threats at greater distances while maintaining a protective posture. This work identifies the advantages of using a non-lens-based, semi-collimated Raman system as compared to traditional methods of obtaining Raman signal at standoff or proximal distances.

The standoff Raman detector that used semi-collimated light to interrogate surface samples showed improved figures of merit at all distances as compared to traditional methods of using lenses to focus laser light to a point. This provides (1) increased flexibility for the Warfighter, whereby they do not need to maintain a fixed distance from the sampling surface; (2) the ability to interrogate larger areas more easily with dispersed analyte on a surface, given the light is not being focused to a small point; and (3) greater ease in maintaining a protective posture because there is more flexibility in the distance that can be used to acquire identifying chemical information.

Blank

CONTENTS

FIGURES

TABLE

STANDOFF RAMAN SEMI-COLLIMATED (SORSC) INSTRUMENT EVALUATION: A COMPARISON TO A TRADITIONAL HANDHELD RAMAN INSTRUMENT

1. INTRODUCTION

Bulk material detection is relatively easy and understandable when approached using spectroscopic based systems. Dispersed material detection is not as easy, although it is necessary, especially when detection techniques are applied at mission-applicable speeds. The difficulties of dispersed material detection are largely based on two requirements: (1) the dispersed materials must physically overlap the transduction technique, and (2) the signal from the analyte must be measured. This is further convoluted by the additional background clutter that occurs when an analyte is very sparsely dispersed, resulting in less analyte available for detection and identification. An example of a dispersed threat may include improvised explosive device residues or disseminated materials released to contaminate an area with potentially harmful chemicals.[1] Use of a proximal detection system is ideal for these types of scenarios;[2] however, proximal detection systems often work only at specific distances, require a lot of power, are heavy, or must be very complicated to achieve flexibility. When a proximal light-based detection system is used on a vehicle, the working distance must be known so that the signal return to the sensor can be optimized.

Light-based sensing techniques are advantageous for proximal or standoff detection because they often do not require direct contact with an analyte to sense it. However, many transduction systems operate only at a specific distance that is based on the optics employed. This issue can be mitigated with the use of adjustable optics that can be automated by coupling them with a distance-measuring instrument. These improvements increase the overall system size, weight, power consumption, and cost.

Raman spectroscopy can include optics with fixed focal lengths at distances of ≥1 m, thereby providing proximal or standoff detection distances when telescopic lenses are used. Typically, Raman data are collected using optics that tightly focus a laser beam to a small spot (<5 mm diameter) in backscatter geometry to maximize the number of Raman scattered photons incident on the detector. This is because Raman is an inherently weak phenomenon. Focusing the laser light maximizes the photon flux incident on the analyte and thereby increases the chance of observing a Raman spectrum. Understanding adequate sampling methods, which are based on the instrument and its physical operation characteristics, can improve maneuverability through contest areas by bounding operational limitations.

Techniques for decreasing the size, weight, power, and cost of an instrument while maintaining maneuverability and operational capabilities are paramount when integrating instrumentation into a Warfighter's gear or onto a vehicle. In this report, a standoff Raman semi-collimated (SORSC) instrument that uses no optics to manage the laser light source is compared to a traditional handheld proximal Raman instrument that uses traditional optics to manage the laser light source. The report documents performance at different distances and angles as well as the capability to sense a dispersed analyte.

2. METHODS

All of the work described herein was performed by personnel from the Chemical Analysis and Physical Properties Branch of the U.S. Army Combat Capabilities Development Command Chemical Biological Center (DEVCOM CBC; Edgewood Area, Aberdeen Proving Ground, MD) from January 2020 through February 2021. All computer-based analysis was completed using MATLAB R2019a software (MathWorks; Natick, MA).

2.1 Instrumentation

2.1.1 Raman Spectrometers

The two Raman spectrometers used throughout this study were 785 nm diode-based Raman systems. Both were handheld instruments designed to be portable (i.e., battery operation compatible), although each system was powered with shore power for the test duration.

The integration time used for all data acquisition through this study was 10 s per spectrum. The 10 s time period was chosen to provide ample signal at a distance of 2 m. A shorter integration time could be used at all distances but at the cost of having a robust, repeatable Raman signal. In all cases, three measurements were obtained: one with the SORSC instrument (Cyclops; Smiths Detection; Edgewood, MD), one with the CBEx system (Snowy Range Instruments; Laramie, WY) when focused, and one with the CBEx system when rastered. These were chosen to identify (1) differences between lens-based and non-lens-based Raman systems and (2) whether the interrogation area affects measurements.

2.1.1.1 SORSC Instrument

The Cyclops SORSC system is a handheld proximal detector that is approximately 4 × 4 × 3 in. Smiths Detection provided the Cyclops as a prototype lens-less Raman system. The system was controlled via an integrated touch screen and a graphical user interface that allows the user to choose an integration time, background subtraction, and library matching. In all cases, the background was subtracted automatically. All data were transferred directly from the instrument to compact disc via a universal serial bus disk drive.

2.1.1.2 Focused Raman System

The lens-based CBEx system is a handheld Raman spectrometer that was obtained from a previous program at DEVCOM CBC. The instrument has two interchangeable telescopic lenses for 1 and 2 m standoff sensing. In addition to the standoff telescopic lenses, the instrument has a cuvette attachment that was not used during this study. The CBEx system could also focus the laser to a single point or "raster" scan it in a circular pattern. The latter provides a larger average area of interrogation for the signal.

The CBEx system was controlled via a tethered laptop computer. Although the CBEx system could be used as a handheld instrument, greater control was possible when the computer provided the shore power and the interface. The CBEx instrument has both high and

low laser power, and the high laser power was used for the duration of this study. As mentioned previously, the spectra were automatically background-subtracted.

2.1.2 Linear and Rotational Stages

Linear and rotational stages from Zaber Technologies (Vancouver, BC) were used to reproducibly reach specific distances or angles for various aspects of this work. A 3 m motorized linear stage (model X-BLQ3000-E01) was used for distance-based measurements to reproducibly attain the same distance point in each trial. A motorized rotational stage (model X-RST120 AK) was used for the rotation-based measurements to reproducibly attain the same angle for each measurement trial. Each stage was controlled by a computer and the company's proprietary control software.

2.2 Interrogation Area

The interrogation area for each system was obtained at both 1 and 2 m. A green paper (Mohawk; no. 104083, BriteHue, 30% recycled, vellum, 8.5 × 11 in., 60 lb) was used to capture digital images of the laser profile on the surface, at the points where data were collected. The green paper was used to help reduce saturation and maximize contrast between the green background and red laser.

A grid scale (American Board of Forensic Odontology [ABFO]; no. 2) was included in each frame so that the actual size of the interrogation area with respect to the pixel size of the digital camera could be determined. The region of interest (ROI) that was chosen in each frame included the scale, which consisted of white areas (background) and dark tick marks. The regions were summed to obtain a two-dimensional intensity representation (intensity per distance) of the two-dimensional spatial region (Figure 2). A fast Fourier transform (FFT) was performed on the data to objectively and reproducibly obtain the frequency of the tick marks and thereby measure the distance between them.

Each image was analyzed as follows to yield an objective and reproducible method of area analysis:

1. Identify the ROI while fully encompassing the incident laser light.
2. Apply Otsu's method to binarize the image to threshold.
3. Suppress structures connected to the border of the image.
4. Morphologically decompose extraneous pixels farther from the border.
5. Measure the properties, including area, of the resulting logical image.

2.3 Analyte Considerations

A polytetrafluoroethylene (PTFE) puck was used for analysis. The puck was 3.5 × 4 × 0.3 cm (width × height × thickness), and it provided a homogeneous material that was not penetrated by any of the laser light. The PTFE puck was mounted onto a bracket that was then secured to either the linear or rotational stage for measurement.

2.4 Spectral Analysis

All spectra were obtained in at least triplicate or from 16 trials. The comparative value between instruments as a figure of merit was identified as the area under the curve (AUC) of the Raman band of interest (721 cm^{-1} symmetric C–C stretch; Figure 1)[3,4] when using PTFE or at 1523 cm^{-1} when analyzing ink on paper. A Lorentzian model[5] was applied to fit the Raman peak of interest:

$$f(x) = \frac{a}{(x-b)^2 + c^2} \tag{1}$$

where a is the peak center, b is the peak width, and c is the full width at half-maximum (FWHM) of the peak.

The AUC was determined for a region of the Raman spectrum that fully included the Raman band of interest. The AUC was fitted using eq 1 and integrated under the fit area. This AUC was used as the comparative metric between distances, instruments, and acquisition techniques. AUC outliers were determined by identifying AUCs that were greater than three scaled median absolute deviations away. If a point was an outlier, that AUC was discarded, and the signal-to-noise ratio (SNR) was determined with the remaining points.

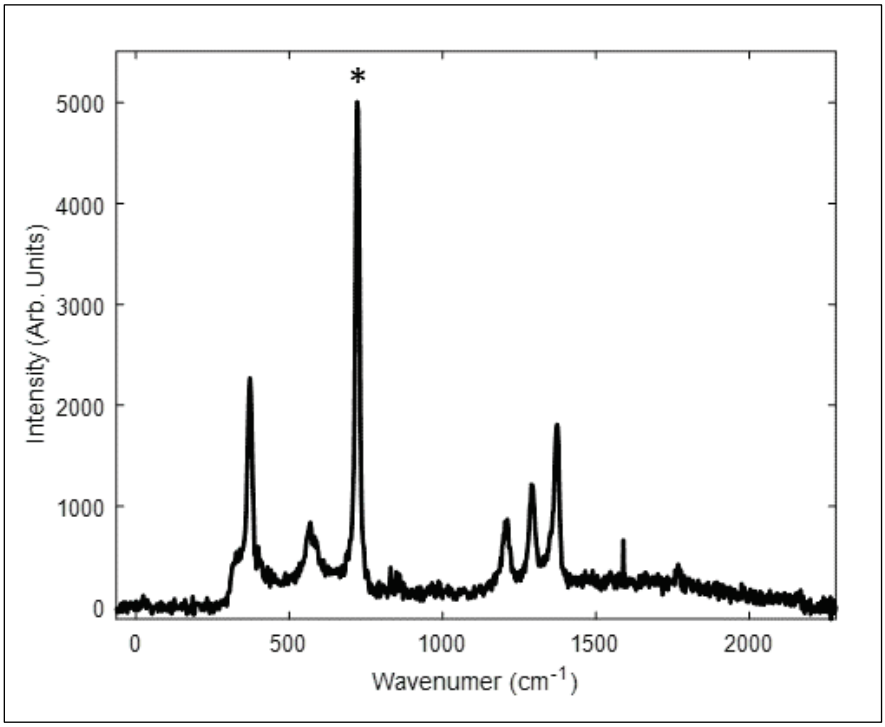

Figure 1. Raman spectrum of PTFE. *Raman band used for comparison purposes throughout this work.

2.5 Distance Dependence Measurements

Distance dependence measurements were completed using a 3 m linear stage (described in Section 2.1.2). Data were obtained with the CBEx instrument in 100 mm increments at the focal region of each lens (focal region ± 1000 mm) and in 500 mm increments outside the focal region. Data with the Cyclops system were obtained in 500 mm increments. The data were obtained in replicate from 3–16 trials at each distance.

2.6 Angle Dependence Measurements

Angle dependence measurements were completed using a rotational stage (described in Section 2.1.2). Data were obtained at distances of 1 and 2 m with a PTFE sample mounted in the center of the rotational stage, perpendicular to the angle of incidence. The appropriate lens was used with the CBEx instrument at each distance, and the Cyclops instrument was used at each distance. Raman spectra were obtained in at least triplicate at 0, 15, 30, 45, 60, and 75° angles.

2.7 Artificial Dissemination Studies

The artificial dissemination studies were performed in two parts. The first part focused on the experimental aspect of creating artificial dissemination patterns and characterizing the instrument's performance with those data. The second part focused on using modeled spectra to characterize each instrument's performance.

Blue ink was printed on white paper to produce artificial dissemination patterns. Spectra were obtained of each pattern, and differences were identified. Calibration curves were completed that were based on 14 increments of ink fill factors, from 100% (solid printed ink) to 0% (only white paper).

3. RESULTS AND DISCUSSION

3.1 Interrogation Area

The imaging area of the two systems, with the appropriate lenses for the CBEx instrument, was used to help determine the areas of integration. This was then used to characterize how each instrument performed the sampling. Because the CBEx instrument has two different settings (e.g., focused vs rastered), the way that area affects the Raman signal can also be evaluated. To objectively determine the area of integration for each system, a digital image was obtained with a scale bar providing millimeter increments (Figure 2A). The remainder of the analysis was completed using MATLAB software to provide the scale and distance per pixel on the digital image, and then image processing techniques were applied to determine the laser integration. Some inconsistencies exist between ABFO no. 2 rulers produced by different manufacturers.[6] However, the methodology described below takes into account the inconstancies of the scale gradations and therefore mitigates any concern of inconsistency.

First, an ROI of the scale bar was chosen (Figure 2B). The pixel intensity was summed per column (if scale bar ROI was on top) or per row (if scale bar ROI was on the side). The summed intensity values provided a patterned signal as shown in Figure 2C. Using FFT, the frequency of the signal was determined, which represents the spatial distance between two low- or high-intensity points (i.e., the tick marks). Figure 2D shows a representative example of an FFT on the signal from the ROI of the scale bar. This example, 0.0201 Hz, represents a spatial separation between the tick marks of 49.75 pixels/mm. As with all data on which an FFT is performed, the Nyquist criterion must be met; the data herein meet this criterion.

Table 1 shows the area for each of the systems at 1 and 2 m. As expected, the raster setting with the CBEx instrument has a greater area than the focused setting, and it provides a larger area of interrogation. In all cases, a larger area of interrogation was realized at greater distances. The laser spot area was between 3 and 3.5 times larger when the system was 1 m farther away. Identifying differences in interrogation area is especially important when analyzing non-bulk samples that may present in a disseminated pattern. A larger area would provide the Warfighter with a greater probability of interrogating an analyte of interest as opposed to the empty space between the analytes.

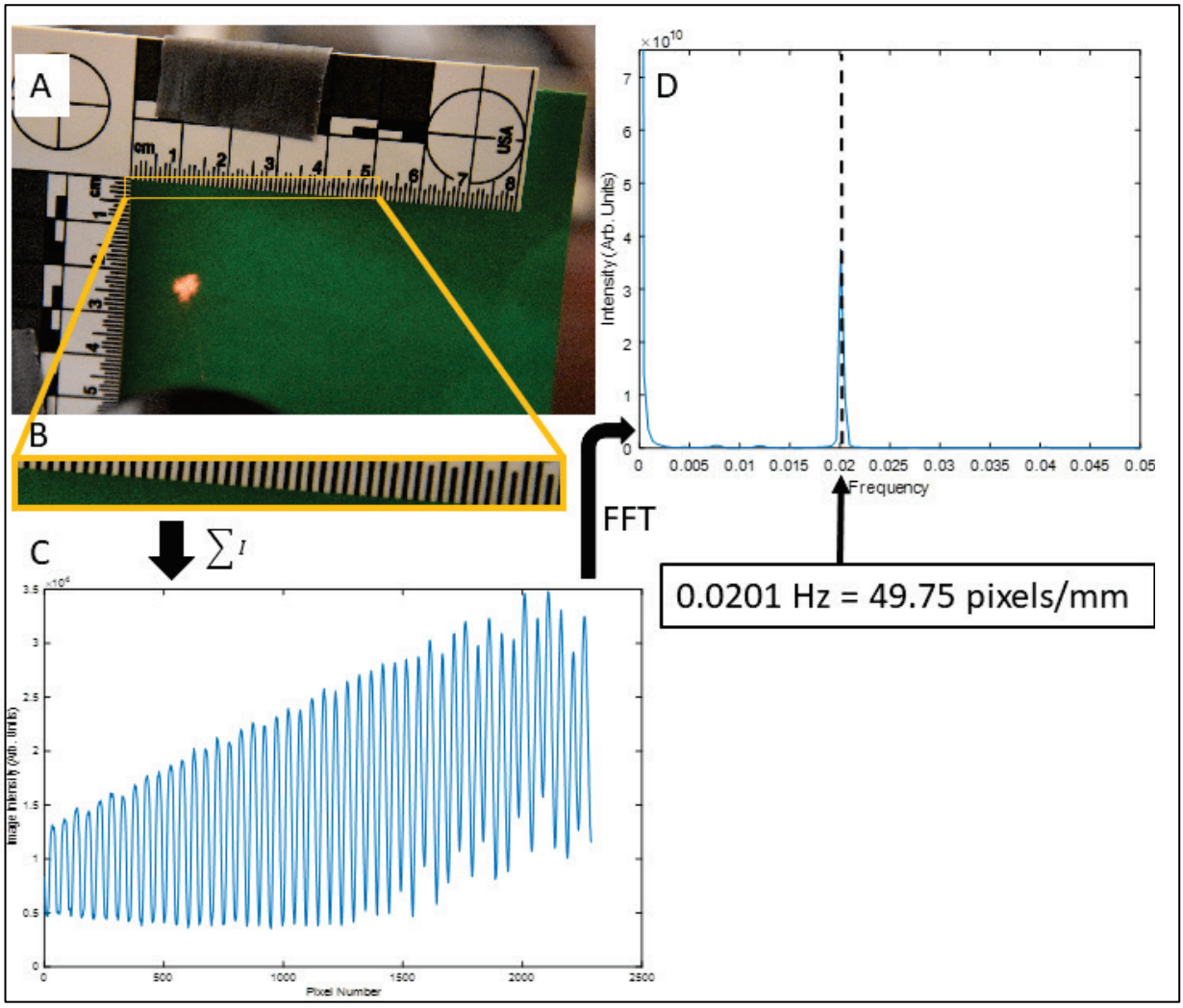

Figure 2. (A) Determining pixel laser spot size via a digital image of the laser spot size with a ruler in the frame; (B) finding an ROI of the ruler markings; (C) gray-scaling and column-wise summing the pixel intensities to create a line profile; and (D) performing an FFT of the spatial profile to accurately determine the resolution of the digital image.

Table 1. Laser Spot Sizes at 1 and 2 m Distances

Integration Distance	Laser Spot Area (mm^2)		
	Cyclops	CBEx Focused	CBEx Rastered
1 m	26.7	2.6	14.9
2 m	78.7	9.4	41.7

3.2 Spectral Analysis

Generally speaking, a Lorentzian model can be used for fitting a Raman band. In some cases, a Gaussian, Gaussian–Lorentzian (GL) sum, or Voigt function can be used, but these are often dependent on the phase or state of the analyte.[5,7] To verify the model for use, Gaussian, Lorentzian, and GL sum models were applied to fit a representative Raman band. A model was chosen based on its goodness of fit (R^2) value and how well the residuals fit (data not shown). Generally, the Lorentzian model provided the best fit for the data. In the instances where the GL sum was a better fit, the difference was marginal. It was determined that a reduction in the number of adjustable parameters outweighed the minor increase in the fit.

The AUC was used to compare differences in the instrumentation. When normalized, the AUC provides a method for comparison between two spectrometers that have comparable spectral resolution. As shown in Figure 3, analysis of variance (ANOVA) tests were used to evaluate the FWHM of the fitted Raman bands to determine the statistical significance between the means of the FWHM values for the different systems and distances. In an ANOVA test, the means of two samples are compared to identify whether they originate from the same mean. As shown in Figure 3, left, all of the 1 m measurements from both systems had means that were not statistically different, and all of the 2 m measurements from both instruments had means that were not statistically different. Furthermore, using a two-way ANOVA test (Figure 3, right) validated this by showing that all of the 2 m measurements originated from a statistically different mean than the 1 m measurements.

The FWHM between the two sets of instruments were not statistically different. The spectral resolution of the two spectrometers is similar. Therefore, although some aspects of the spectrometers were unknown, these systems could be compared with one another using the AUC. The AUC provides an area measurement that can be used as a figure of merit between the two instruments.

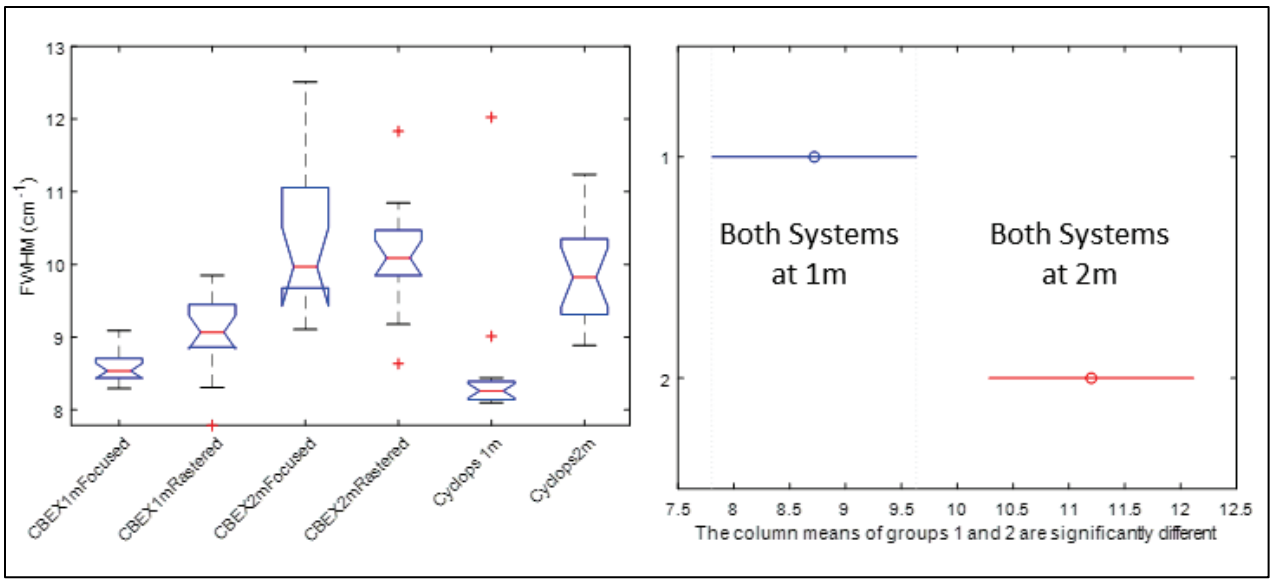

Figure 3. ANOVA analysis of FWHM of the 721 cm^{-1} Raman band of PTFE. (Left) Box plot shows the means and spread of the FWHM from the data at 1 and 2 m for each instrument. (Right) Two-way ANOVA test shows the spectral resolution was different (but comparable) between 1 and 2 m.

3.3 Distance Dependence Measurements

The distance dependence between the two instruments was expected to be different, largely because a focusing lens was used for the CBEx instrument. The lens requires a focal region as an ideal area for obtaining the backscattered Raman signal. This requires the CBEx instrument to be within a certain range of the lens' focal region and results in distance dependence of the instrument. However, another aspect of the instrument distance dependence was evaluated; namely, the sensitivity of the signal changed with small, incremental changes in distance.

In an effort to understand this and ensure that the AUC was adequately fitting each of the Raman peaks in the spectra, the R^2 for each trial at each distance was recorded. This is an empirical visual representation of how well the function fit the band. That is, as the amplitude of the Raman band decreases, the goodness of fit also decreases because of the increased noise; eventually, when the signal is at about the noise level, the function is very poorly representative of the data manifesting itself through a reduction of the R^2 values. In Figure 4A, the CBEx data show high confidence in the goodness of fit (≥0.9) at 1 m for the focused and raster scanned 1 m lens (black and red dots, respectively). There is also a high confidence in the goodness of fit (≥0.9) for the focused and raster scanned 2 m lens (black and red asterisks, respectively). The decrease in the goodness of fit and, therefore, an indication of poor fit quality (due to lower signal) is shown for the 1 m lens at approximately 1.5 m and greater and for the 2 m lens at less than 1 m, where the R^2 values consistently drop well below 0.9. The data for the Cyclops system show adequate fitting (≥0.9) in all measurements out to 3 m (Figure 4B). The model appears well fit to the data around the focal regions, thereby providing confidence in identifying the sensitivity of moving off peak.

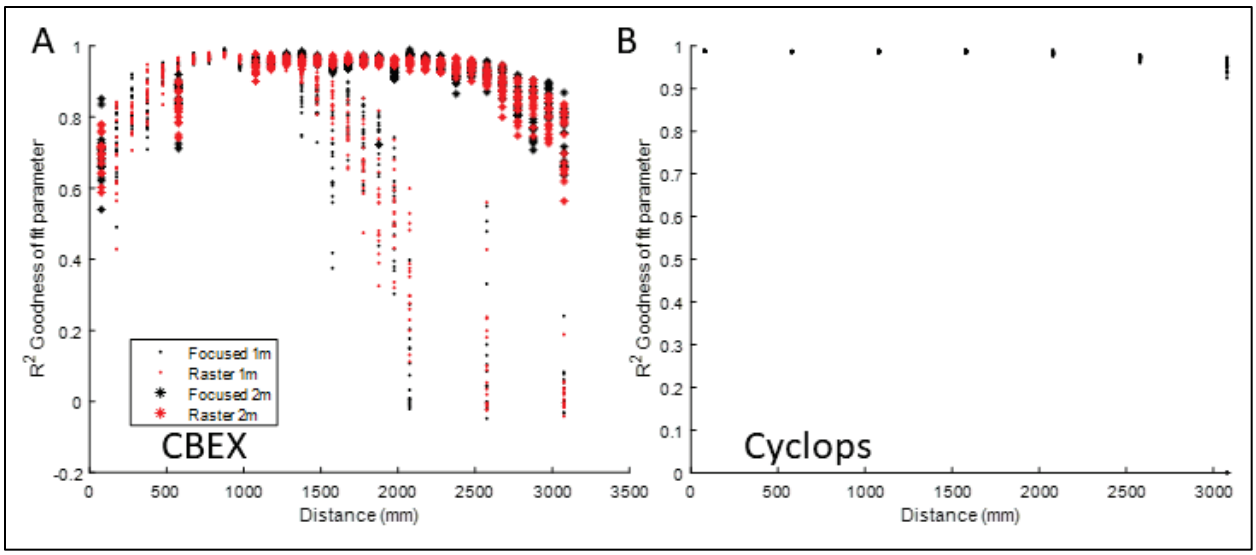

Figure 4. A visual representation of the R^2 goodness of fit of the AUC at the 721 cm^{-1} Raman band for the (A) CBEx and (B) Cyclops instruments. R^2 values of 1 are perfectly fit, whereas R^2 values of <0.9 are considered not well fit for the purpose of this report.

3.3.1 Distance Dependence of Each Instrument

The distance dependence of the Cyclops instrument is not dependent on the lens focal region. Therefore, it can be fit to a model to determine the signal, AUC, or SNR at arbitrary distances. Figure 5A shows the distance dependence of the Cyclops system from 0 to 3 m. The distance (d) dependence of the signal decreases with $1/d^{1.3}$, which is a slower decrease in signal than occurs with the expected inverse-square relationship. As shown in Figure 5A, the strongest signal can be obtained when closest to the analyte, whereas the weakest signal is obtained farther away. An "optimal" distance was not determined in this study; however, a minimum distance could be determined for each analyte with specific acquisition parameters. By not being reliant on the focal region of a lens, the Warfighter has more flexibility in their positioning relative to the analyte of interest. This has the potential to improve soldier survivability and, in turn, increase soldier lethality.

As expected, the CBEx instrument has a focal region that provides higher relative intensity of the Raman backscatter than occurs in regions outside the focal region (Figure 5B). It is clear from the data that the signal is focal region dependent. The 1 m lens had a narrower focal region, as shown by the sharpness of the data peak at approximately 1 m (Figure 5B, blue and red lines). In contrast, the 2 m lens appeared to have a broader focal region (Figure 5B, yellow and purple lines). This too was expected because the numerical aperture (NA) for standoff lenses tends to be lower; the focal point is farther from the lens, which necessitates a shallower angle and results in a lower NA. The broader focal region provides for more flexibility in distance for the Warfighter during operation of the handheld system, although its optimal performance is within the focal region. As the instrument is forced to the extremes away from the focal region, its performance deteriorates.

When the Cyclops and CBEx instruments are compared, the Cyclops provides greater flexibility. The CBEx instrument performs best at the focal region, which may be difficult for the Warfighter to precisely acquire, whereas the Cyclops instrument's performance increases as the analyte is brought closer to the spectrometer. This suggests that the Warfighter's confidence in measurement can be increased as the potential target is brought closer to the instrument.

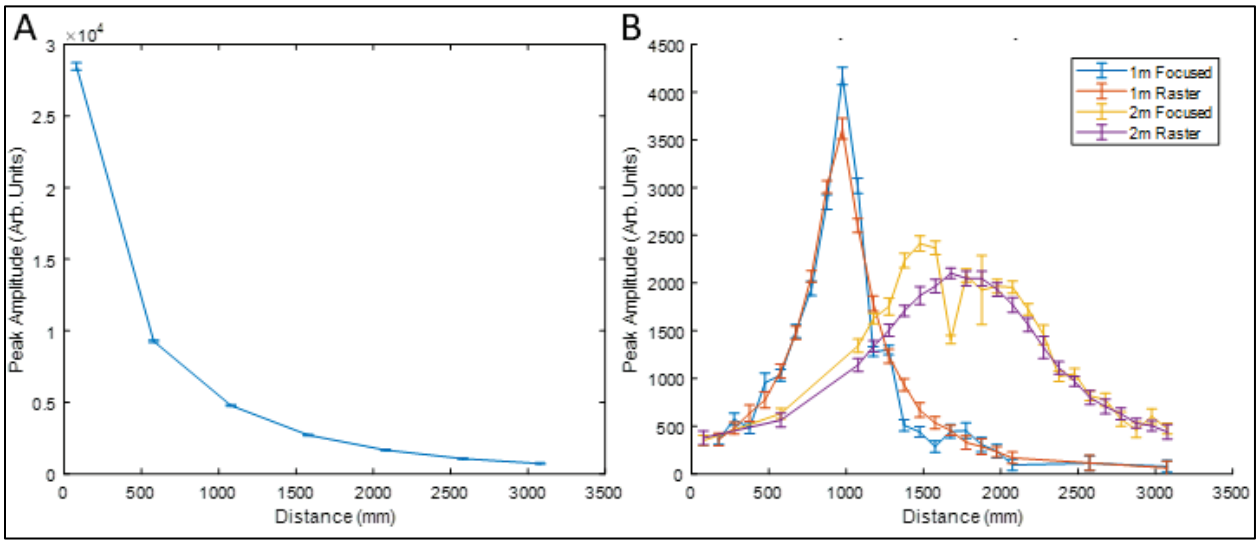

Figure 5. Distance dependence of the (A) Cyclops and (B) CBEx instruments.

3.3.2 AUC at 1 and 2 m

The AUC is an appropriate method for comparing these methodologies when the spectral data has been normalized; therefore, this can be used to determine how well the instruments perform at different distances. The AUC indicates that, at 1 and 2 m, the Cyclops instrument outperforms the CBEx instrument, despite this being the focal region for the respective CBEx lenses. As shown in Figure 6A, the AUC of the Cyclops instrument at 1 m is almost two times larger than that of the CBEx focused method and about three times larger than that of the rastered method. At 2 m (Figure 6B), the AUC of the Cyclops instrument is more than three times larger than that of the CBEx instrument for both the focused and the rastered methods. The measurement variation of the AUC does increase with the Cyclops instrument from 1 to 2 m, although it remains statistically significantly higher in all cases as compared to the CBEx instrument.

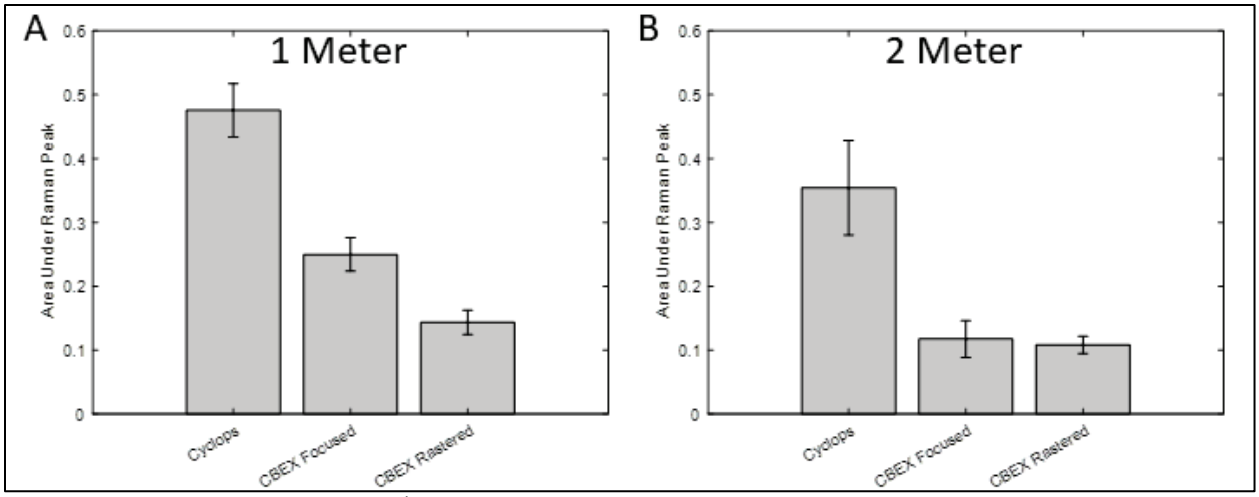

Figure 6. AUC of the 721 cm^{-1} Raman band at (A) 1 m and (B) 2 m for the unfocused, focused, and rastered methods.

3.4 Angle Dependence Measurements

Angle dependence measurements were made to assess the need to hold the instrument perpendicular to a surface to obtain chemical measurements at proximal distances. The angle dependence of Raman signals is well known,[8,9] but the extent that it applies to nonfocused Raman is not known. Therefore, a preliminary assessment was made of the angle dependence of nonfocused Raman scatter compared to that of focused and rastered techniques. Figure 7 shows the angle dependence of the AUC. The Cyclops (nonfocused) Raman scatter at 1 m had a stronger distance dependence than the other techniques at any other distances. For all of the instruments, the AUC decreased as the angle was increased. The largest change in the AUC was when the instrument was moved from perpendicular to 75°; it occurred for the Cyclops instrument at 1 m at about two times the magnitude of signal of any of the other collected data. However, the Cyclops instrument at 2 m behaved similarly to the other instruments.

In addition to the obvious distance dependence shown for the nonfocused technique (the Cyclops instrument) at 1 m, the AUC at 75° was, within error, as good or better than that for all of the other techniques when perpendicular at any distance or angle. The angle dependence is due to two primary phenomena. First is the inherent Raman scattering profile, whereby forward and backscatter are preferential; and second is the solid collection angle of the optics or openings, which are used to collect or allow light into the spectrometer. Because the same angles were employed here, the effects inherent to Raman scattering are the same. Therefore, the effects of the optics (or the lack of optics) are likely the basis for the differences in the angle dependence. The greater effect observed at 1 m aligns well with our hypothesis; with no optics, the collection cone will be widest when the spectrometer is closest to the sample. Because scatter is minimized perpendicular to the path the light travels, the 1 m proximal detection with no optics would likely exhibit minimized scattering compared to other optics that are designed to have an appropriate working distance.

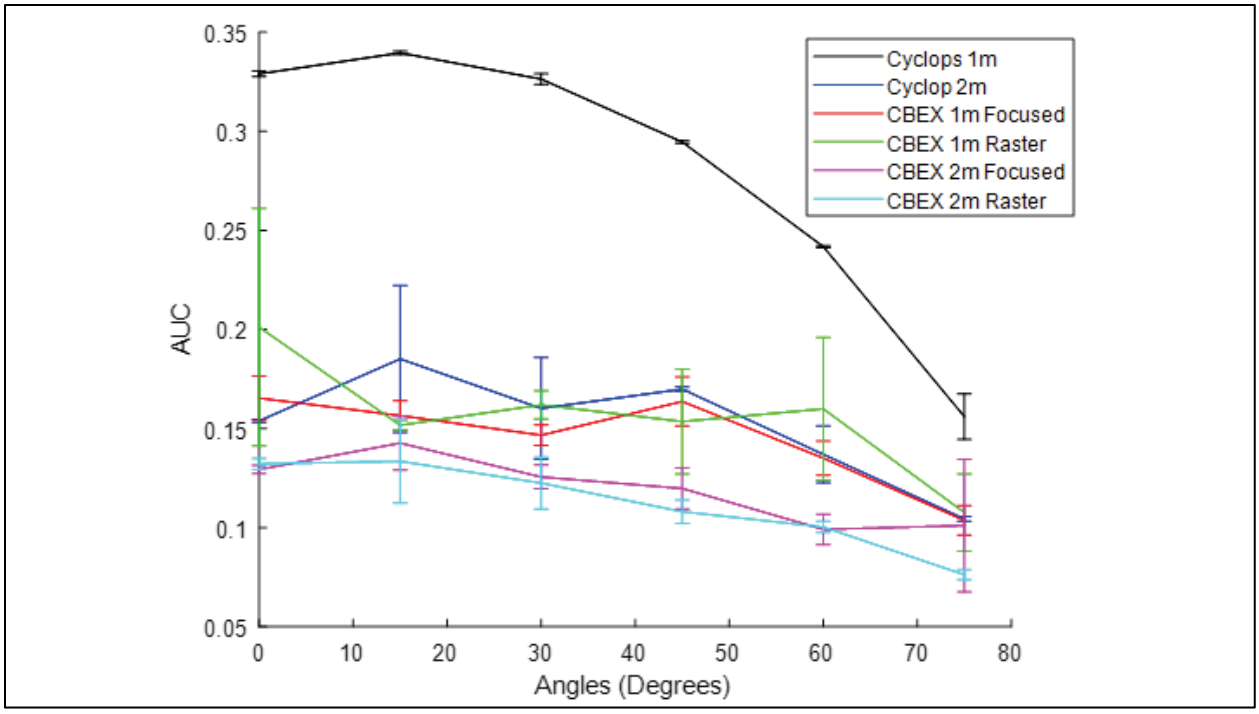

Figure 7. Angle dependence measurements of the Cyclops instrument at 1 m (black line) and 2 m (blue line), the CBEx instrument when focused at 1 m (red line) and 2 m (magenta line), and the raster scan at 1 m (green line) and 2 m (cyan line).

3.5 Simulation and Modeling Studies

3.5.1 Laser Profile Simulation

Laser profiles were estimated and simulated to compare analyte overlap with predicted and experimental data. An inkjet printer was used to produce varying droplet densities to simulate material coverage on a surface. Using the same simulated droplet pattern for simulations and experiments makes them directly comparable.

The laser profiles were simulated and assumed to be circular. On average, this assumption was valid, as indicated by the data listed in Table 1. The simulated laser profiles are shown in Figure 8. The left side of Figure 8 is a single circular laser profile (red, L) that overlaps with circles for analytes A, B, and C. This was valid (not scaled) for the Cyclops (nonfocused) instrument and the CBEx instrument that employs focusing optics. The simulated laser profile fully overlapped analyte A, partially overlapped analyte B, and did not overlap analyte C at all. The right side of Figure 8 represents the toroid profile produced by the CBEx instrument that uses raster scanning. The laser profile is represented by the red ring (L1) with the center removed (green, L2). This profile partially overlaps with analyte B and does not overlap with analytes A or C. These profiles were scaled and used based on the technique being simulated.

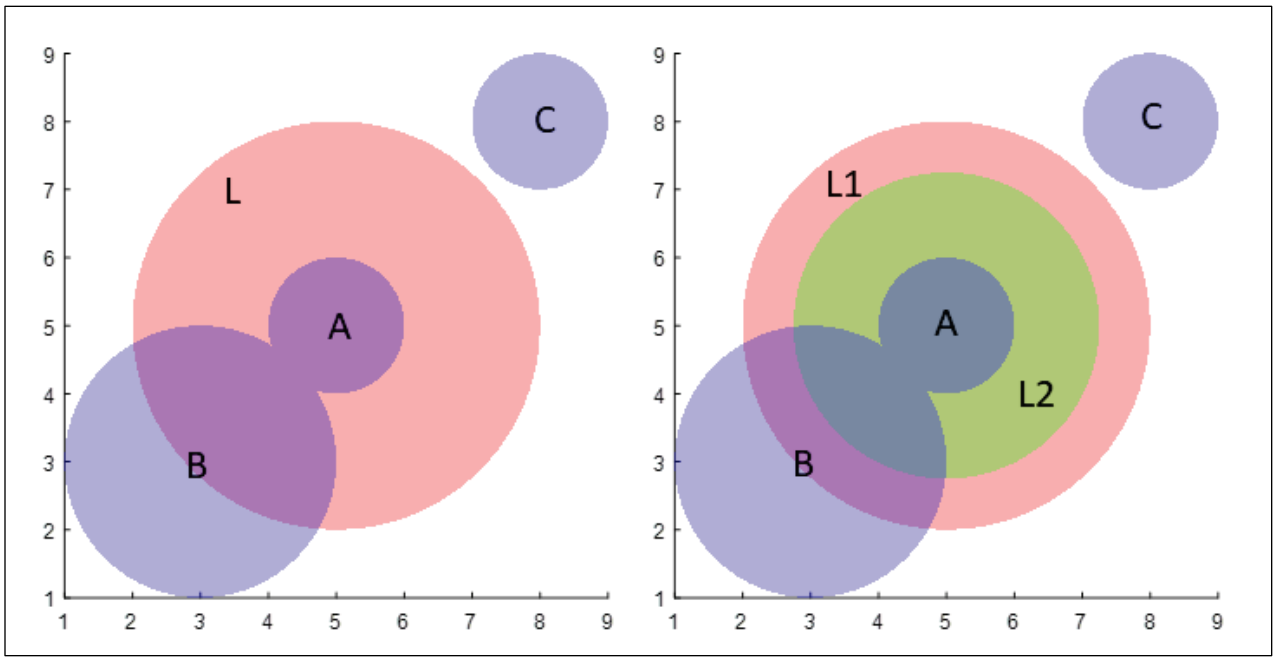

Figure 8. Simulated laser profiles (not scaled for individual techniques). (Left) A solid red circle represents the laser (L) with analytes A, B, and C and approximates the nonfocused and focused proximal lasers. (Right) Raster profile (red, L1) with the center taken out (green, L2) overlapping analytes A and B.

3.5.2 Simulated Droplet Experiments

Blue ink can be used to print simulated disseminations in relevant patterns on paper so that system performance for disseminated materials can be determined. An inkjet printer was used to print areas with varying fill factors of blue ink on white paper. As shown in Figure 9A, the ink fill factor ranged from 100% (solid blue box) to 0% (blank white paper). The different fill factors were used as a calibration to determine the response to the amount of blue ink present. The spectra in Figure 9B show that the profiles are differentiable: peaks that can be identified from the blue ink are not present in the white paper (circa 1500 cm^{-1}).

The different ink densities were printed into 2 × 2 in. blocks on white copy paper and used as target analytes. The same pattern was also simulated with ink (the blue ink spectrum from Figure 9) and white copy paper (the white paper spectrum from Figure 9). The spectra were summed and normalized to represent how they would be collected and then analyzed the same way for both the experimental and the simulated data. The data are shown in Figure 10. There was good agreement between the distribution of the area (percentage of area filled with ink in the 2 × 2 in. block), represented as the solid black line; the simulated signal that was determined by overlap of the simulated laser beam (described in Figure 8); the printed droplet pattern (red dashed line); and the experimental data obtained with the Cyclops instrument. There was agreement at both 1 and 2 m, which suggests that as the distance is increased, these relationships will hold true.

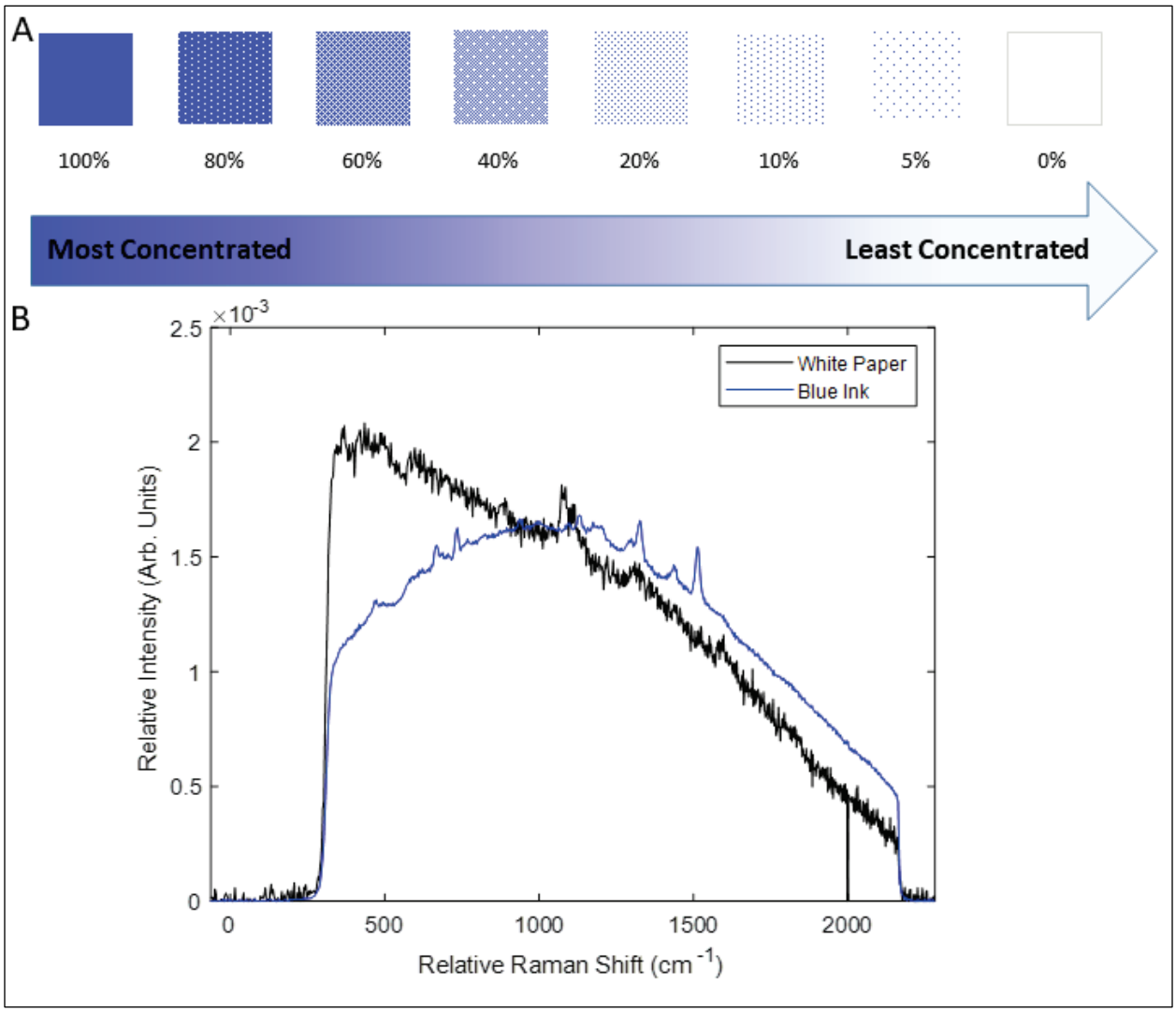

Figure 9. (A) Fill factor profiles of ink printed on white paper from most concentrated (100%) to least concentrated (0%, blank); and (B) spectra of white paper (black line) and blue ink (blue line).

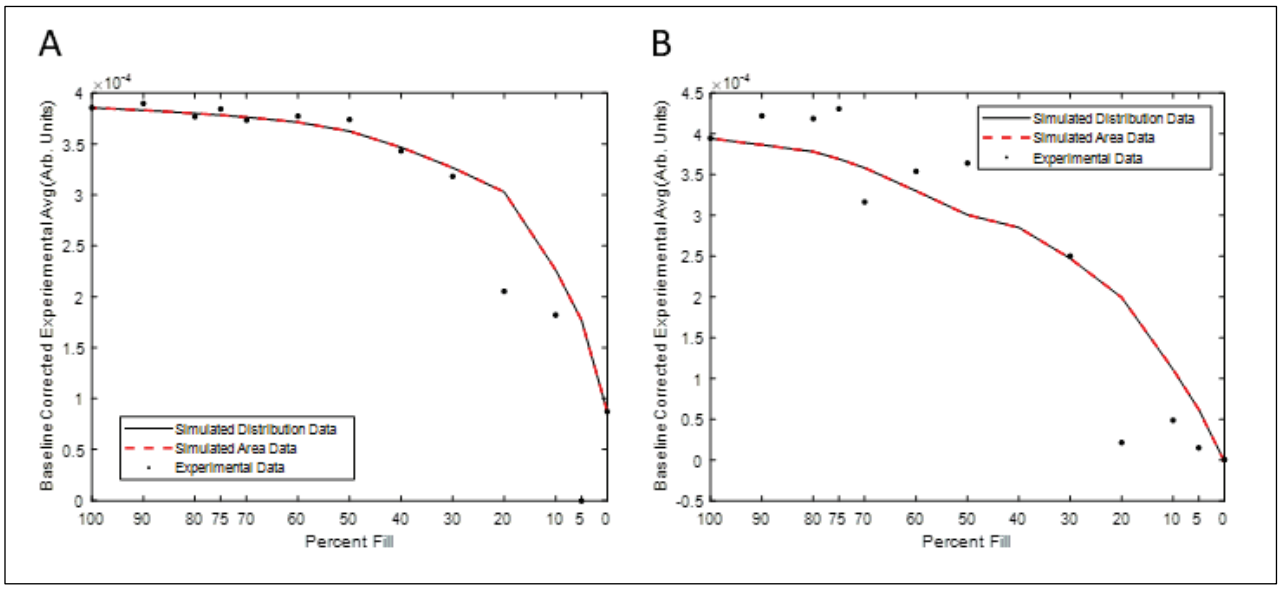

Figure 10. Nonfocused Raman with varying fill factors of blue ink printed on paper (black points), the estimated percentage fill based on the density (black line), and the simulated spectral signal (red dashed line) for (A) 1 m and (B) 2 m.

The agreement between these data suggest that this simulated density, simulated spectral analysis, and spectral analysis of experimental data can all be related for other purposes as well. Extending this simplified model of spectra summation, the assumption is made that the two materials (analyte and background) are opaque. Informing the model through acquisition of pure material and pure background with the same experimental conditions would include taking into account some differences, such as differences in Raman cross sections.

4. CONCLUSION

The SORSC (Cyclops) instrument performs as well as or better than a traditional method of obtaining proximal Raman spectra. One key difference is there is no focal region, which provides greater flexibility for the Warfighter when obtaining spectra or greater capability when the system is operated on a vehicle. Although the total signal tended to decrease with distance, the total signal obtained was comparable to that of the focused-based Raman system at its ideal working distance. These results suggest that removing the optics and relying only on a collimated or semi-collimated source reduces size, weight, power, and cost of an instrument and functionally increases the capability of employing Raman technologies in the field.

LITERATURE CITED

1. Wilcox, P.G.; Emmons, E.D.; Pardoe, I.J. *Raman Spectra and Cross Sections of Chemical Warfare Agents, Agent Simulants, and Explosives Using 213 nm Deep-Ultraviolet Laser Excitation*; ECBC-TR-1512; U.S. Army Edgewood Chemical Biological Center: Aberdeen Proving Ground, MD, May 2018; UNCLASSIFIED Report (AD1051864).

2. Chirico, R.; Almaviva, S.; Colao, F.; Fiorani, L.; Nuvoli, M.; Schweikert, W.; Schnürer, F.; Cassioli, L.; Grossi, S.; Murra, D.; Menicucci, I.; Angelini, F.; Palucci, A. Proximal Detection of Traces of Energetic Materials with an Eye-Safe UV Raman Prototype Developed for Civil Applications. *Sensors* **2016,** *16* (1), 8.

3. Peacock, C.J.; Hendra, P.J.; Willis, H.A.; Cudby, M.E.A. Raman Spectrum and Vibrational Assignment for Poly(tetrafluoroethylene). *Journal of the Chemical Society A: Inorganic, Physical, Theoretical* **1970,** 2943–2947.

4. Bower, D.I.; Maddams, W.F. *The Vibrational Spectroscopy of Polymers*. Cambridge University Press: Cambridge, UK, 1992.

5. Yuan, X.; Mayanovic, R.A. An Empirical Study on Raman Peak Fitting and Its Application to Raman Quantitative Research. *Applied Spectroscopy* **2017,** *71* (10), 2325–2338.

6. Ferrucci, M.; Doiron, T.D.; Thompson, R.M.; Jones, J.P.; Freeman, A.J.; Neiman, J.A. Dimensional Review of Scales for Forensic Photography. *Journal of Forensic Sciences* **2016,** *61* (2), 509–519.

7. Bradley, M. *Curve Fitting in Raman and IR Spectroscopy: Basic Theory of Line Shapes and Applications;* Application Note 50733; Thermo Fisher Scientific: Madison, WI, 2007.

8. Nafie, L.; Stein, P.; Fanconi, B.; Peticolas, W.L. Angular Dependence of Raman Scattering Intensity. *The Journal of Chemical Physics* **1970,** *52* (3), 1584–1588.

9. Nafie, L.A. Theory of Raman Scattering. In *Handbook of Raman Spectroscopy: From the Research Laboratory to the Process Line;* Lewis, I.R., Edwards, H.G.M., Eds.; Practical Spectroscopy Series Vol. 28; Marcel Dekker: New York, 2001, pp 1–10.

Blank

ACRONYMS AND ABBREVIATIONS

ABFO	American Board of Forensic Odontology
ANOVA	analysis of variance
AUC	area under the curve
DEVCOM CBC	U.S. Army Combat Capabilities Development Command Chemical Biological Center
FFT	fast Fourier transform
FWHM	full width at half-maximum
GL	Gaussian–Lorentzian
NA	numerical aperture
PTFE	polytetrafluoroethylene
R^2	goodness of fit
ROI	region of interest
SNR	signal-to-noise ratio
SORSC	standoff Raman semi-collimated

DISTRIBUTION LIST

The following individuals and organizations were provided with one electronic version of this report:

U.S. Army Combat Capabilities Development Command Chemical Biological Center (DEVCOM CBC)
FCDD-CBR-CP
ATTN: Languirand, E.
Ellzy, M.
McDaniel, P.

DEVCOM CBC Technical Library
FCDD-CBR-L
ATTN: Foppiano, S.
Stein, J.

Defense Technical Information Center
ATTN: DTIC OA


U.S. ARMY COMBAT CAPABILITIES DEVELOPMENT COMMAND
CHEMICAL BIOLOGICAL CENTER